



LUND UNIVERSITY

Performance and wear mechanisms of novel superhard diamond and boron nitride based tools in machining Al-SiCp metal matrix composite

Bushlya, Volodymyr; Lenrick, Filip; Gutnichenko, Oleksandr; Petrusha, Igor; Osipov, Oleksandr; Kristiansson, Stefan; Stahl, Jan Eric

Published in:
Wear

DOI:
[10.1016/j.wear.2017.01.036](https://doi.org/10.1016/j.wear.2017.01.036)

2017

Document Version:
Early version, also known as pre-print

[Link to publication](#)

Citation for published version (APA):

Bushlya, V., Lenrick, F., Gutnichenko, O., Petrusha, I., Osipov, O., Kristiansson, S., & Stahl, J. E. (2017). Performance and wear mechanisms of novel superhard diamond and boron nitride based tools in machining Al-SiCp metal matrix composite. *Wear*, 376-377, 152-164. <https://doi.org/10.1016/j.wear.2017.01.036>

Total number of authors:
7

General rights

Unless other specific re-use rights are stated the following general rights apply:
Copyright and moral rights for the publications made accessible in the public portal are retained by the authors and/or other copyright owners and it is a condition of accessing publications that users recognise and abide by the legal requirements associated with these rights.

- Users may download and print one copy of any publication from the public portal for the purpose of private study or research.
- You may not further distribute the material or use it for any profit-making activity or commercial gain
- You may freely distribute the URL identifying the publication in the public portal

Read more about Creative commons licenses: <https://creativecommons.org/licenses/>

Take down policy

If you believe that this document breaches copyright please contact us providing details, and we will remove access to the work immediately and investigate your claim.

LUND UNIVERSITY

PO Box 117
221 00 Lund
+46 46-222 00 00

Performance and wear mechanisms of novel superhard diamond and boron nitride based tools in machining Al-SiCp metal matrix composite

Volodymyr Bushlya^{a*}, Oleksandr Gutnichenko^a, Filip Lenrick^a, Igor Petrusha^b, Oleksandr Osipov^b, Stefan Kristiansson^c, Jan-Eric Stahl^a

^a*Division of Production and Materials Engineering, Lund University, 221 00 Lund, Sweden*

^b*Department of Synthesis and Sintering of Superhard Materials, Institute for Superhard Materials, 04074 Kiev, Ukraine*

^c*Amtek Components Sweden AB, Aspenäsgatan 2, 521 51 Flöby, Sweden*

Abstract

Metal matrix composites are the desired materials in aerospace and automotive industries since they possess high specific strength. However addition of reinforcement to the matrix material brings the adverse effects of high wear rate of tool materials used in their machining. The current study addresses the issues of wear and performance of superhard tools when high speed machining cast Al-Si alloy reinforced with particulate SiC (20% vol.). A wide range of developed superhard materials was compared to the commercial PCD tools. Nano grain sized wBN-cBN, binderless cBN; B₆O-cBN, nano-diamond with WC binder; diamond/MAX-phase; and diamond/SiC tool materials were employed. Tool wear tests involved dry machining at cutting speeds 200 and 400 m/min at fixed cutting length of 14 000 meters. Use of nano-diamond/WC and diamond/MAX-phase composites resulted in their rapid deterioration due to primarily adhesive pluck-out of diamond and binder phase. Diamond/SiC material exhibited slightly lower performance than the PCD, with the primary wear being the abrasive on the SiC binder phase. Machining with cBN-based tooling at lower speed lead to formation of stable build-up layer, frequently accompanied by severe seizure of tool and workpiece material. However at speed of 400 m/min the absence of such build-up layer caused rapid tool wear. In case of PCD and diamond-SiC tooling build-up layer remained stable in the whole cutting speed range. Presence of chemical and diffusional wear mechanisms for this tooling has been confirmed through scanning and transmission electron microscopy. Archard-type model of abrasive tool wear was developed for modelling of tool deterioration for all studied tool materials.

1. Introduction

Metal matrix composites (MMC) are a relatively new class of materials that have a variety of advantageous properties like high specific strength, wear resistance, hardness, etc. They have found application in aerospace, automotive and other industries. The most widespread, due to the cost benefits, class of MMC has aluminum alloy matrix strengthened by ceramic (eg. Al₂O₃, SiC, B₄C, etc.) reinforcement [1]. It is the reinforcement that brings favorable properties but introduces the main problem in machining the MMC materials related to rapid wear of cutting tools and poor machinability.

Conventional tooling like high speed steel, cemented carbides and ceramics, which hardness is lower than the reinforcement, suffer from severe abrasion [2]. Polycrystalline cubic boron nitride (PCBN) tools with low cBN content and polycrystalline diamond (PCD) tools were found to be roughly one and two orders of magnitude better in wear resistance than cemented carbide [2]. That is why superhard diamond or cubic boron nitride (cBN) tooling pose scientific and industrial interest. This is explained by the high hardness of such tooling which can be ranked as follows: for PCD the hardness is $HV = 70-85$ GPa; for PCBN with high cBN content it equals $HV = 36-40$ GPa; and for PCBN with low cBN content the hardness is $HV = 28-32$ GPa [3]. The hardness for all these materials exceeds the value for SiC reinforcement thus allowing for reduced wear rate.

PCBN grades with binders that are softer than the wear resistant cBN phase, mainly AlN [2] or TiC [4, 5], have been tested. The tool wear is characterized mainly by abrasion or abrasion combined with adhesion of workpiece material [4]. MMC machining with PCBN having low cBN content additionally exhibited edge chipping and nose fracture [5]. The use of binderless cBN with ultra-fine grain microstructure, which gives improved hardness, has shown only 20-30% improvement in wear resistance, when compared to PCBN with ceramic binders [5]. However, tooling with coarse grain microstructure is known to have better wear resistance and generate finer surface roughness [6, 7]. Therefore binderless cBN with coarser grain-size might have improved wear resistance.

Machining of MMC is frequently accompanied by adhesion of workpiece material and formation of build-up edge that introduces protective action against abrasion by SiC reinforcement. Muthukrishnan et al. [7] have shown that PCD machining at low cutting speed was accompanied by significant

formation of BUE which was attributed to increased tool life at this cutting speed. BUE acted as a protective cap on the cutting edge. Similar effect was found when machining Al-SiC_p MMC with PCBN tools. Ciftci I. et al. [4] have shown that PCBN machining with cutting speed of $v_c = 150$ m/min results in large and strongly attached BUE. The dimensions of BUE reduced at increased cutting speed and lead to accelerated tool wear. Adhesion of the MMC and formation of BUE varies with the tool material. PCBN tools have a stronger tendency to adhesion than PCD tools [5]. In general, superhard tool materials of different composition show individual sensitivity to abrasive and adhesive wear mechanisms and therefore different wear resistance when machining MMC. Therefore evaluation of performance for any novel superhard materials is of scientific and practical interest.

The aim of this study is to evaluate the performance and obtain in-depth understanding of wear mechanisms of several novel diamond- and cBN-based superhard tooling in comparison to commercial PCD. Binderless cBN, wBN-cBN, B₆O-cBN, nano-diamond with WC binder, diamond with MAX-phase binder, and diamond-SiC tool materials were tested. Wear characteristics of the tooling was examined via 3D optical, scanning electron, transmission electron microscopy, and energy dispersive X-ray analysis. Archard-type model of abrasive tool wear is developed for modelling of tool deterioration.

2. Experimental setup

The following metal matrix composite (MMC) material was used in experiments – AlSi9Mg0.3 aluminum alloy reinforced with SiC particles (20% vol.) having the grain-size of 10 to 30 μm . The molten Al-SiC_p MMC material was gravity cast (directly from the industrial furnace, Amtek Components Sweden AB) into tubular stainless steel moulds. The moulds were allowed to cool for 30 seconds on air and then rapidly cooled in a water basin. This sequence was found to minimize the sinking of SiC particles and provide the MMC microstructure identical to the industrial one (see Fig. 1). Cast MMC ingots were pre-machined to bars of 56 mm in diameter and 400 mm in length prior to the actual machining tests.

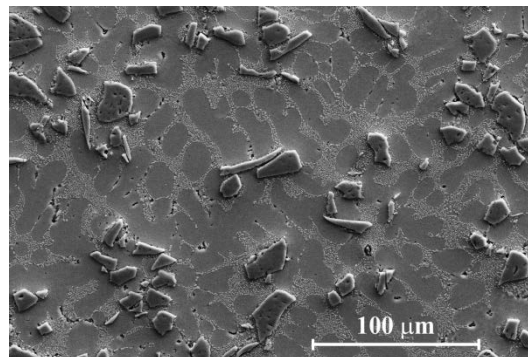
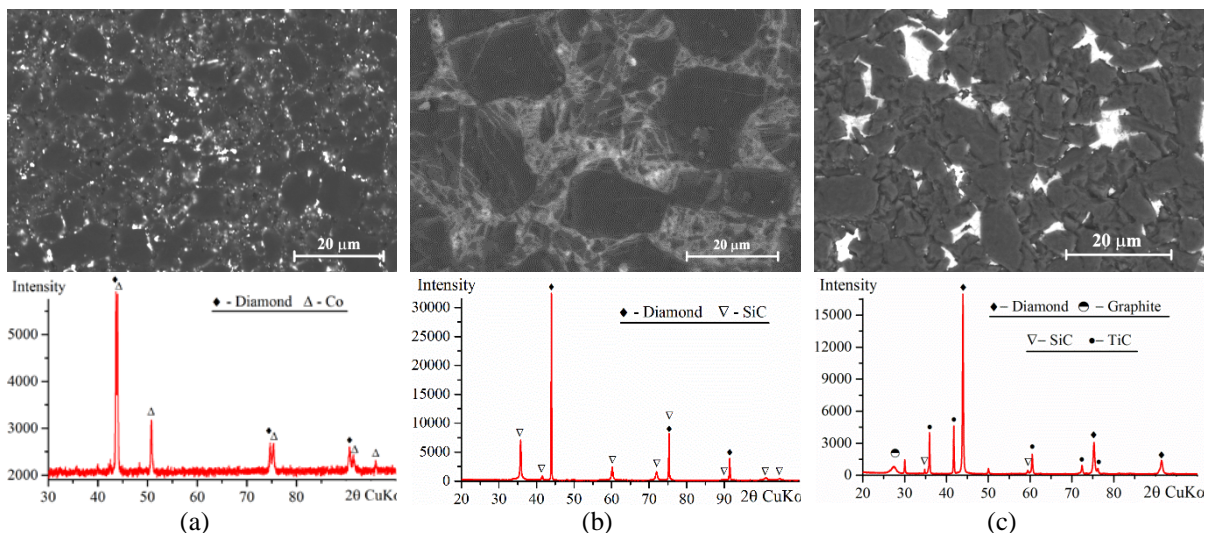


Fig. 1. Scanning electron microscope (SEM) image of the microstructure of Al-SiC_p MMC workpiece material.

The machining test involved longitudinal turning operation where the commercial PCD reference tool material was compared to several experimental superhard tool materials. Some of the materials structurally are also polycrystalline diamond (PCD) compacts and therefore binder type is used in material designation to avoid confusion between various PCD materials. The description of all tooling materials, their properties, microstructure and phase content are listed below.

1. D-Co – commercial polycrystalline diamond material which forms a solid diamond matrix as a result of intergrowth of diamond grains. The formation of strong diamond-to-diamond bonding is a result of dissolution-precipitation sintering mechanism when molten cobalt dissolves part of the diamond grain to the solubility limit of carbon in the Co-C solution and precipitates it as diamond on the diamond grains (Fig. 2.a). The material possesses high hardness of $HV = 89$ GPa (Fig. 3), high fracture toughness ($K_{IC} = 9.8 \text{ MPa}\cdot\text{m}^{1/2}$) and thermal conductivity of $k = 760 \text{ W}/(\text{m}\cdot\text{K})$ [3].

2. D-SiC – thermostable polycrystalline composite which forms as a result of infiltration of molten silicon into the diamond preform and subsequent reaction of both phases with formation of silicon carbide matrix (Fig. 2.b). The material has hardness of $HV = 84$ GPa (Fig. 3), lower toughness of $K_{IC} = 7.6$ MPa·m^{1/2} and lower thermal conductivity of $k \approx 200$ W/(m·K) [8].
3. D-MAX₉₅ – experimental polycrystalline diamond material where the bonding of diamond is realized via decomposition of Ti₃SiC₂ MAX-phase during the sintering, release of TiC, elemental silicon and titanium and their subsequent reaction with the diamond [9]. Mixture of 95 vol.% diamond and 5 vol.% Ti₃SiC₂ was subjected to the sintering process (Fig. 2.c). The sintering resulted in a material with hardness of $HV = 71$ GPa (Fig. 3).
4. D-MAX₆₀ – similar experimental polycrystalline diamond material which contained 60 vol.% diamond and 40 vol.% Ti₃SiC₂ prior to the sintering (Fig. 2.d). Reduced diamond contents, compared to D-MAX₉₅, resulted in a lower hardness of $HV = 62$ GPa (Fig. 3).
5. nD-nWC – experimental material for which the nano-diamond (3-15 nm) is subjected to sintering with tungsten [10], the reaction products creating a nano-grained WC matrix (Fig. 2.e). Residual surface oxygen introduces an undesired by-product of WO₂. Softer WC matrix and presence of WO₂ cause a reduced hardness of $HV = 52$ GPa (Fig. 3).
6. bcBN – experimental binderless cubic boron nitride material which possesses a solid cBN matrix as a result of diffusional bonding of cBN grains during the high temperature – high pressure sintering (2300 °C and 8 GPa). Additive of 3 vol.% of silicon nitride (Fig. 2.f) is introduced to the cBN matrix for enhancement of fracture toughness ($K_{IC} = 12.6$ MPa·m^{1/2}) [11]. The material has highest hardness of $HV = 54$ GPa and thermal conductivity of $k = 180$ W/(m·K) [12] among the boron nitride based tooling.
7. wBN-cBN – experimental superhard material which forms as a result of controlled partial transformation (50 vol.%) of ultra-fine grain wurtzite boron nitride to a cubic one in the region of thermodynamic stability of cBN at pressure 8 GPa and temperature of 1700 °C (Fig. 2.g). While the mechanical properties are rather high (Fig. 3), its thermal conductivity is only $k = 26$ W/(m·K) [13].
8. B₆O-cBN – experimental superhard material which combines superhard cBN grains bound in a superhard matrix of boron sub-oxide B₆O. The mixture of 40 vol. % B₆O and 60 vol.% cBN were sintered at pressure 8 GPa and temperature of 2000 °C (Fig. 2.h) [14]. High hardness of the material is combined with rather low fracture toughness ($K_{IC} = 4.7$ MPa·m^{1/2}) and low thermal conductivity of $k = 14$ W/(m·K) [14].



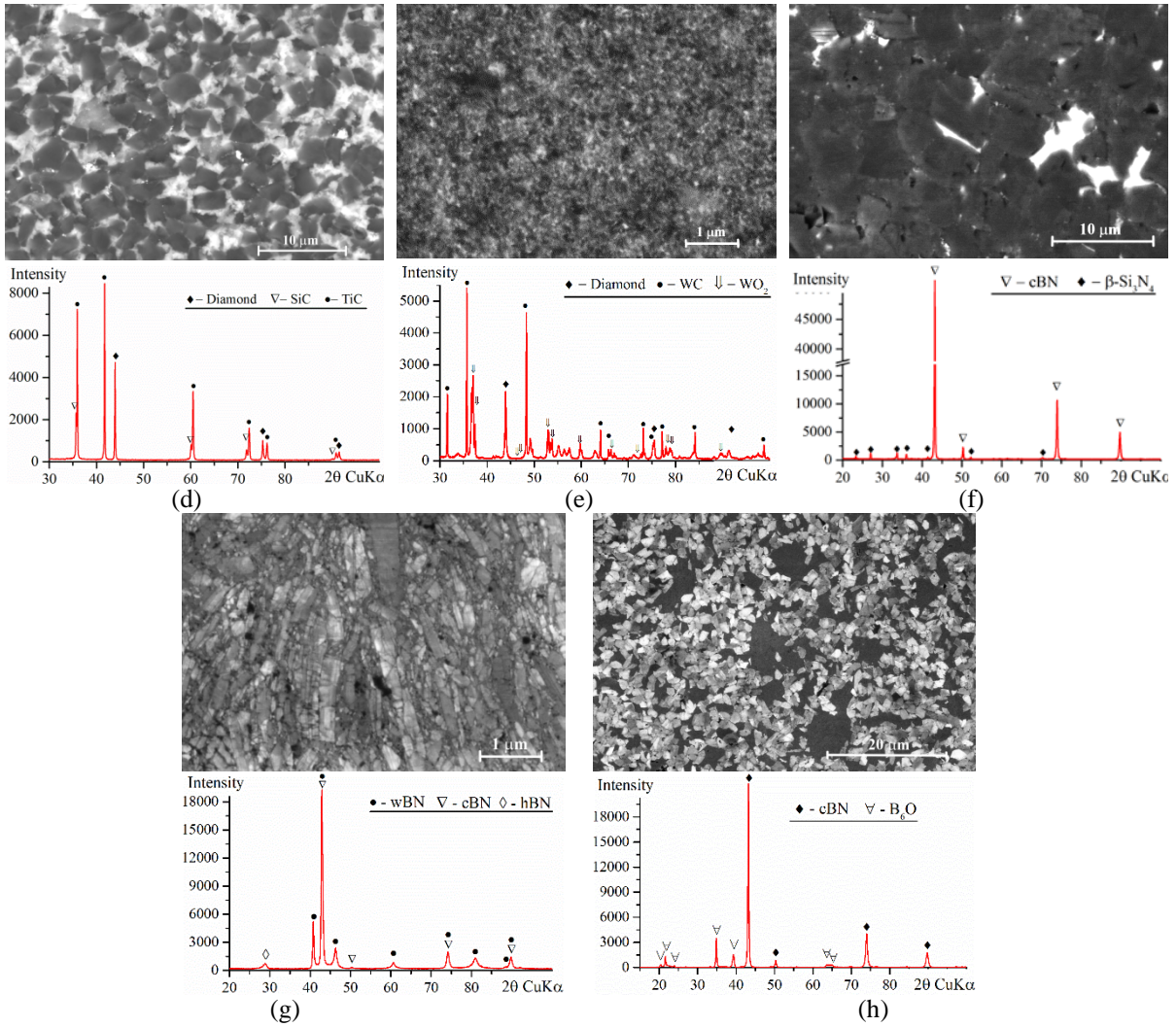


Fig. 2. SEM images of the microstructure and corresponding XRD pattern for tool materials: (a) D-Co, (b) D-SiC, (c) D-MAX₉₅, (d) D-MAX₆₀, (e) nD-nWC, (f) bcBN, (g) wBN-cBN, (h) B₆O-cBN.

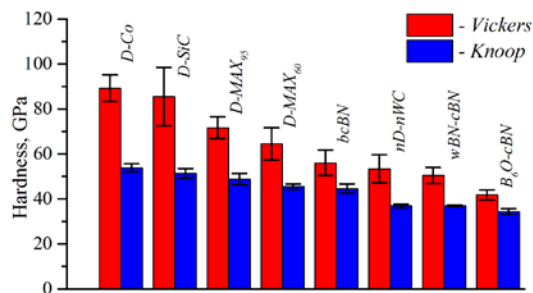


Fig. 3. Vickers and Knoop hardness of the tool materials.

Round inserts RNGN090300E15 with nominal edge radius of 15 μm were placed on CRSNL3225P09 toolholder, which provided -6° back and -6° side rake angles. Cutting conditions corresponded to a finishing operation where feed rate and depth of cut were kept constant $f = 0.15 \text{ mm/rev}$ and $a_p = 0.3 \text{ mm}$, while two cutting speeds, $v_c = 200 \text{ m/min}$ and 400 m/min , were employed. All tests were conducted under dry machining conditions, since coolant application reduces tool life [2]. Tests were interrupted when either tool wear reached $VB = 300 \mu\text{m}$ or the total tool engagement distance equaled approximately 14 000 meters.

Cutting forces were continuously recorded with Kistler 9129AA dynamometer, while tool wear and surface roughness were regularly inspected after 500 – 600 meters of machining. Leica MZ16 stereomicroscope was used for the measurement of flank wear VB , while Alicona InfiniteFocus 3D optical microscope was used for 3D analysis of worn tools. LEO/Zeiss 1560 high resolution scanning electron microscope (SEM) was used for the detailed inspection of the tool and workpiece material microstructure, worn tools, machined surface and sub-surface. FEI NanoLab 600 dual beam microscope was used for lamella preparation using focused ion beam (FIB) lift-out technique [15]. JEOL 3000F transmission electron microscope (TEM) was used for imaging, selected area electron diffraction (SAED) and energy dispersive X-ray (EDX) analysis (SDD X-Maxⁿ EDX system, Oxford Instruments). XRD analysis of tool materials was done on STOE Darmstadt diffractometer with $\text{CuK}\alpha$ source. Hardness of the tool materials was measured with Vickers and Knoop indenters at load 4.9 N (see Fig. 3) on Ernst Leitz Wetzlar microhardness tester.

3. Results

3.1. Tool wear

Fig. 4 shows the development of the flank wear VB for all tool materials at both cutting speeds employed. Based on the results of the tests, the materials can be grouped into high- and low-performance ones. Fig. 4.b shows that both diamond-based materials with MAX-phase binders and the nano-diamond tooling reached the tool life criterion of $VB = 300 \mu\text{m}$ within the first 2500 – 3000 meters of tool engagement. All other tool materials (Fig. 4.a) were tested for the engagement of 14 000 meters. It can be seen that the increase in the cutting speed from $v_c = 200 \text{ m/min}$ to 400 m/min results in the increases of the tool wear for the high-performing tooling. On average, 50 % to 100 % intensification of the tool wear is attributed to the increased cutting speed.

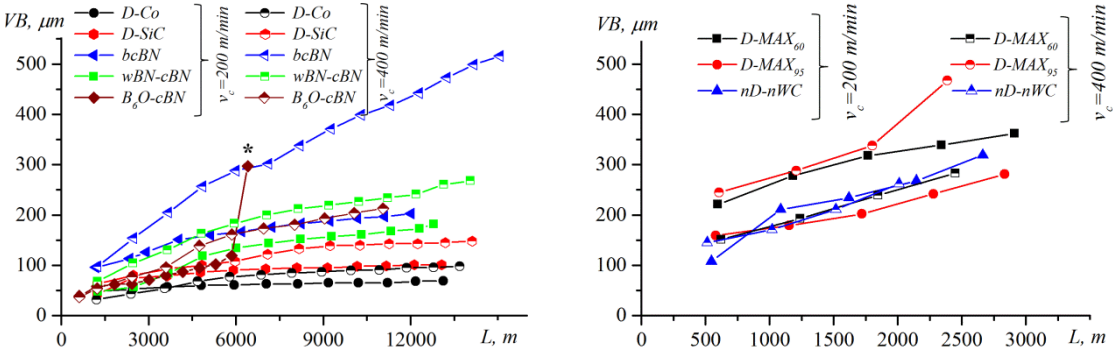


Fig. 4. Tool wear development when machining with (a) high performance and (b) low performance tooling.

Fig. 5 presents the tests results in terms of linear wear rate ($LWR, \mu\text{m}/\text{km}$), defined as the ratio of the tool wear to the engagement distance measured within the normal wear region. It shows that D-Co material, the hardest among the tested (Fig. 3), possesses the highest wear resistance. The same relation is observed for D-SiC tool material that is the second hardest (Fig. 3), which follows the trend typical for abrasive wear. However the other diamond based materials have extremely low wear resistance due to, as shown later, intensive adhesive wear. The expected relation between the tool material hardness and the wear resistance was not directly followed for cBN-based materials either. wBN-cBN and B₆O-cBN tools showed lower linear wear rates at $v_c = 400 \text{ m/min}$ than that harder binderless cBN tool grade. This is related to the stable adhesion of the MMC workpiece material to the tool contact surfaces, mostly the rake, for these grades and protection of the tool against the abrasion of the incoming SiC particles. Even more intensive adhesion of the MMC to the tool surfaces for wBN-cBN and B₆O-cBN at lower cutting speed of $v_c = 200 \text{ m/min}$ (Fig. 22.b) resulted in flaking and chipping on the tool rake as indicated on Fig. 5.

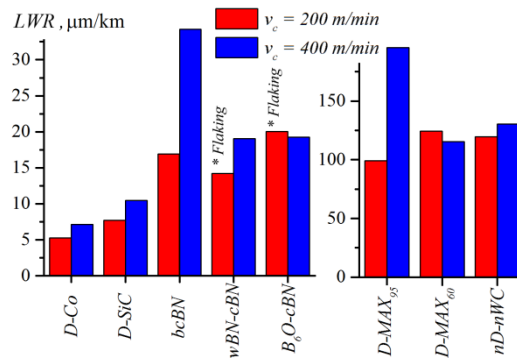


Fig. 5. Linear wear rate (LWR) for different tool materials.

Analysis of the worn tools has shown that D-MAX₉₅, D-MAX₆₀ and nD-nWC low-performing grades experienced both the flank wear and the crater wear. High-performing grades, on the opposite, were characterized by the flank wear and only bcBN experienced slight crater wear at cutting speed of $v_c = 400 \text{ m/min}$ (Fig. 6) which is related to the complete removal of protective workpiece layer that adheres to the tool surfaces in all other cases. Such stable adhesion of the tool protection layer (TPL) covered the wear surfaces and made it difficult to characterize them. Therefore an ultrasonic-assisted etching in 10% NaOH solution, in order to remove the TPL, was done after detailed microscopic inspection of the tools in as-worn state.

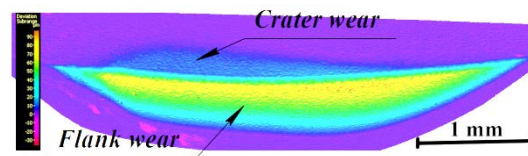


Fig. 6. Results of 3-D volume difference measurement for bcBN tool ($v_c = 400 \text{ m/min}$).

Subsequent analysis of the worn tools with the help of 3D microscopy has revealed that flank and crater wear do not completely characterize the wear topography. The original edge radius of $r_\beta = 15 \mu\text{m}$, identical for all tools, changed in the course of tool wear, as illustrated on Fig. 7. Apart from the edge radius, clearance angle α_{VB} (Fig. 7.a) was also found to deviate from its nominal value, which for the given insert and toolholder geometry should equal $\alpha_o = 9.7 \text{ deg}$. [16]. Fig. 7 shows that a negative clearance angle is forming on the D-SiC tool, while bcBN grade attains the theoretical value.

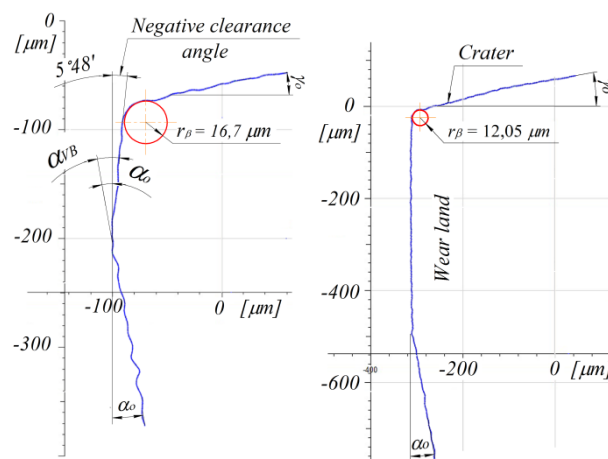


Fig. 7. Cross-sectional data for the worn (a) D-SiC and (b) bcBN tools ($v_c = 400 \text{ m/min}$).

Fig. 8 summarizes the results of the measurement of edge radius r_β and clearance angle α_{VB} for different tool materials and test conditions. It shows that D-Co and D-SiC materials, which have the highest performance, form a highly negative clearance angle. This negative clearance angle is observed on the

etched tools, while the same measurement done prior to the etching indicates that the angle is on the level of the nominal one. This indicates that the workpiece material layer is adhering to the tool flank of D-Co and D-SiC tool and also acts as the tool protection layer (TPL) against the abrasion by SiC particles, which is also discussed later in the article. For other tooling materials the TPL was observed only on the rake.

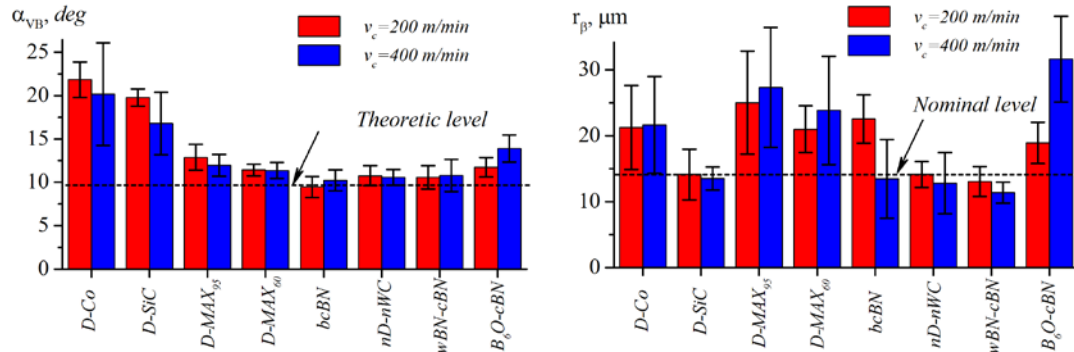


Fig. 8. Measurement results of (a) clearance angle and (b) edge radius for worn tools.

Formation of the negative clearance angle and presence of crater wear for several grades indicate that both the flank wear VB and linear wear rate LWR do not completely characterize the intensity of the wear process and that the volumetric changes should be accounted for. Volume difference measurement (VDM) module of the 3D microscope was used for such analysis. The VDM method calculates the difference between the surfaces of new and worn tool in the same location as exemplified for bcBN tool in Fig. 6. Fig. 9 summarizes the calculated results of the volumetric wear rate (VWR , mm^3/km) determined with the use of VDM method. It can be seen that diamond tool materials with MAX-phase binder have high wear rate which has minor dependence on the cutting speed. This is related to the adhesive pluck out of the diamond grains and binder (see Fig. 10.a) due to poor binding between these phases. For other materials the wear surfaces have smoothed appearance with apparent scratches due to abrasive wear, as exemplified for the D-SiC tooling shown on Fig. 10.b. Fig. 10.b also shows that diamond phase attained minimal abrasive damage while the softer SiC binder has been preferentially abraded from the tool rake.

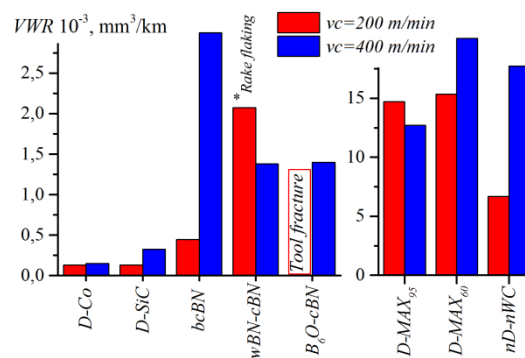


Fig. 9. Volumetric wear rate (VWR) for different tool materials.

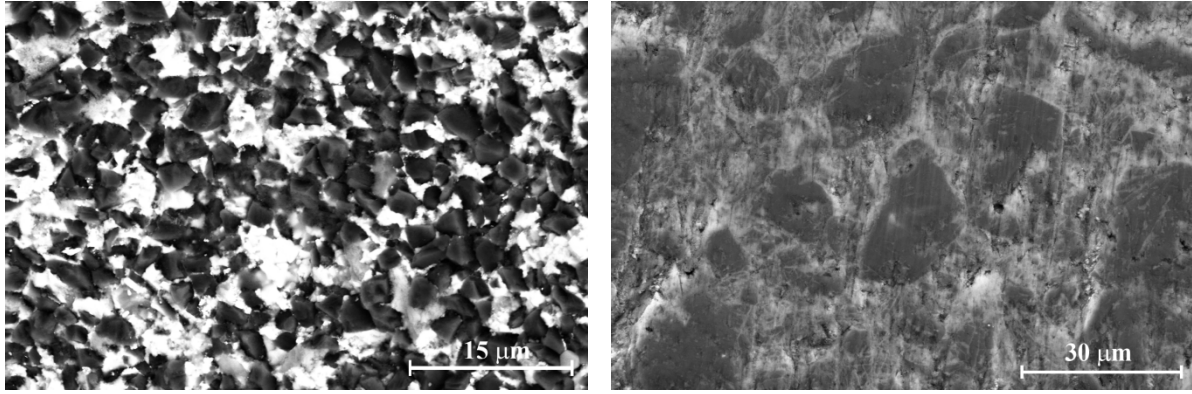


Fig. 10. SEM images of non-etched worn rake surface for (a) D-MAX₆₀ and (b) D-SiC at $v_c = 200$ m/min.

The dramatic difference in the volumetric wear rate (VWR) for machining at $v_c = 200$ m/min and $v_c = 400$ m/min with bcBN tooling is related to the changes in formation and retention of the tool protective layer that forms due to built-up of workpiece material on the tool surfaces. Fig. 11.a shows that the entire rake of the bcBN tool is covered with the TPL at $v_c = 200$ m/min, yet only a minor workpiece adhesion outside the cutting area is observed in the case of $v_c = 400$ m/min. Continual microscopic observations for the case of $v_c = 400$ m/min have shown that only a slight TPL was forming on the tool at the initial engagement, but was destabilized and removed in the course of machining with the progression of tool wear. For all other high-performing tool materials the TPL was maintained at all test conditions, even though the stability and dimensions of the TPL were decreasing at increased higher speed.

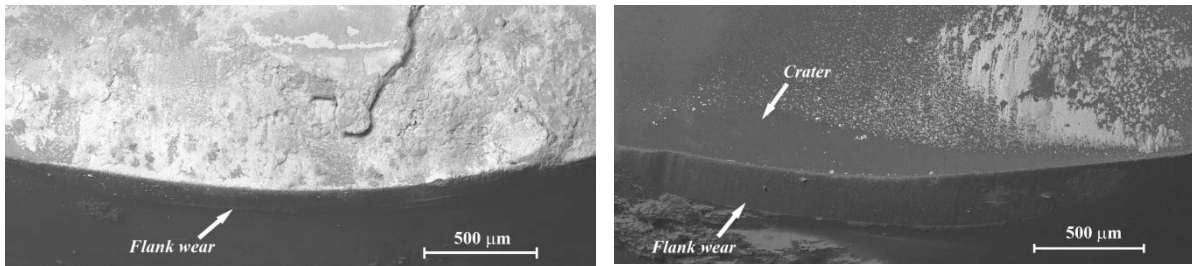


Fig. 11. SEM images of bcBN tools worn at cutting speed (a) $v_c = 200$ m/min and (b) $v_c = 400$ m/min.

3.2. Modelling of tool wear

The observations on the tool wear presented above indicate that abrasive wear mechanism is the dominant within this study. Modelling and prediction of abrasive wear between the components of dissimilar hardness is dominated by the use of Archard wear model [17] that is originally notated as follows:

$$W = \frac{K}{H} \cdot P \cdot S$$

where W – volume of removed softer material, K – wear constant, H – material hardness, P – normal force, and S – traveled distance.

This Archard wear model can be presented in the following formulation that applies to the flank wear of a cutting tool.

$$A_w \cdot b = \frac{K}{H_{tool}} \cdot N_{cl} \cdot e, \quad \text{Eq. 1.}$$

where A_w – cross-sectional wear area (Fig. 12.c), b – active length of the cutting edge (Fig. 12.a), H_{tool} – hardness of the tool material (Fig. 3), N_{cl} – normal force acting on the clearance (Fig. 12.b), and e – tool engagement distance.

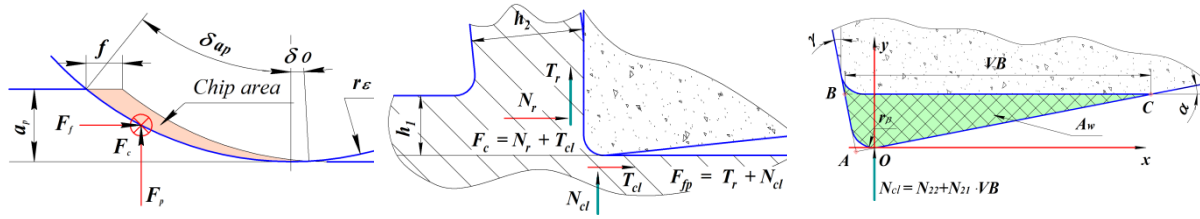


Fig. 12. Schematic of (a) cutting forces acting on a tool, (b) decomposition of forces acting on the rake and clearance for a new tool, (c) normal force N_{cl} on the worn clearance and respective wear area A_w .

For an insert with the nose radius r_ϵ or a round one, the cutting force component F_{fp} located in the AR direction [18] contains the tangential force acting on the rake T_r and normal force acting on the clearance N_{cl} (Fig. 12.b) and can be determined according to the following equation:

$$F_{fp} = \sqrt{F_f^2 + F_p^2} = T_r + N_{cl}. \quad \text{Eq. 2.}$$

The normal force on the clearance N_{cl} for a new cutting tool can be identified by extrapolation of the F_f and F_p forces to the zero chip thickness [19], i.e. the moment when the tangential component T_r equals zero. Figure 13 shows an example of recorded cutting forces for machining MMC with the new D-Co tool at cutting speed $v_c = 200$ m/min when the feed was continuously increased from 5 to 60 $\mu\text{m}/\text{rev}$. The Figure 13 indicates that up to the feed of $f \approx 15$ $\mu\text{m}/\text{rev}$, which corresponds in our case [20] to the maximum theoretical chip thickness of $h_{1max} = 4.9$ μm , the force components remain constant and represent the actual cutting forces acting only on the tool clearance.

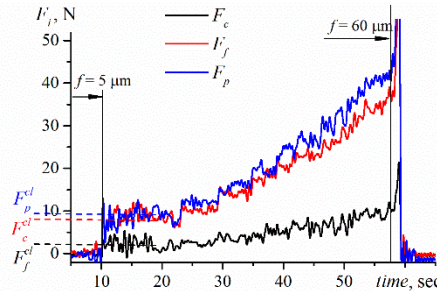


Fig. 13. Development of cutting forces while continuously increasing feed ($f = 5 - 60$ $\mu\text{m}/\text{rev}$) for new D-Co tool ($v_c = 200$ m/min).

The normal force of the tool clearance can then be computed as:

$$N_{cl} = \sqrt{(F_f^{cl})^2 + (F_p^{cl})^2}, \quad \text{Eq. 3}$$

while the force component F_c^{cl} (Fig. 13) represents the tangential force on the clearance T_{cl} .

Both the N_{cl} (Eq. 3) and the T_{cl} forces found for a new tool are increasing with the development of the tool wear VB . Considering the absence of any significant crater wear, meaning that T_r and N_r force components (Fig. 12.b) are fixed, the increase of the cutting forces F_c , F_f , and F_p in the course of the tool wear can be only attributed to the progression of wear VB , as exemplified for bcBN tool (Fig. 14).

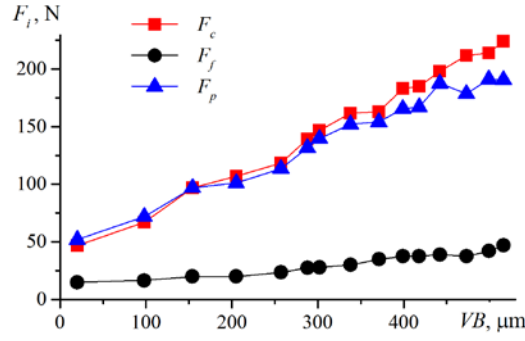


Fig. 14. Development of cutting forces with the wear for bcBN tool ($v_c = 400$ m/min).

Combination of Eq. 2 and Eq. 3 with the force vs. VB data similar to ones on Fig. 14 allows determination of the influence of the wear on the force F_{fp} . Fig. 15.a shows the examples of such calculated influence for the case of D-Co and D-SiC tool when machining MMC with $v_c = 400$ m/min. The slope of the line (Fig. 15.a) describes the influence of the tool wear and therefore the normal force on the clearance for worn tool can be calculated as:

$$N_{cl} = N_{22} + N_{21} \cdot VB,$$

where N_{22} is the value for new tool (Eq. 3) and N_{21} is the tangent of the slope angle (see Fig. 15.a). Similarly, the tangential force can be described as $T_{cl} = T_{22} + T_{21} \cdot VB$.

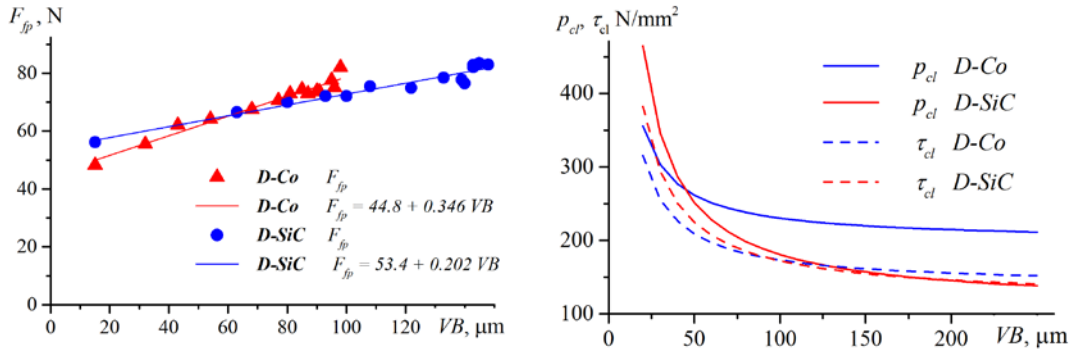


Fig. 15. (a) Resultant force component F_{fp} and (b) respective average normal pressure p_{cl} and tangential stress τ_{cl} on the tool clearance as a function of wear land VB for D-Co and D-SiC ($v_c = 400$ m/min).

The average normal pressure p_{cl} and the average tangential stress τ_{cl} that are acting on the clearance and respectively wear land can be accordingly determined as:

$$p_{cl} = \frac{N_{cl}}{VB \cdot b} = \frac{N_{22} + N_{21} \cdot VB}{VB \cdot r_\epsilon \cdot \left(\arccos\left(\frac{r_\epsilon - a_p}{r_\epsilon}\right) + \arcsin\left(\frac{f}{2 \cdot r_\epsilon}\right) \right)},$$

$$\tau_{cl} = \frac{T_{cl}}{VB \cdot b} = \frac{T_{22} + T_{21} \cdot VB}{VB \cdot b}.$$

Figure 15.b illustrates the influence of tool wear on the determined contact stresses for machining with D-Co and D-SiC tools. It can be seen that the contact stresses in both cases are reducing with the increase of VB , yet for D-SiC tool such reduction is more pronounced. This should be attributed to the larger edge radius r_β and negative clearance angle α_{VB} that develop on the D-Co tool in the course of tool wear (Fig. 8) and the associated larger forces acting on the clearance possessing similar VB .

When including a more detailed account of tool geometry – rake angle γ , clearance angle α , and edge radius r_β – Archard wear model (Eq. 2) can be written in the following form:

$$\frac{(VB^2 - VB \cdot r_\beta) \cdot \cos(\alpha) \cdot \sin(\alpha)}{2} \cdot b = \frac{K \cdot (N_{22} + N_{21} \cdot VB) \cdot e}{H_{tool}} \quad \text{Eq. 4}$$

Solution of this Eq. 4 with respect to the flank wear VB provides a tool for modeling the development of tool wear over the tool engagement distance e .

Figure 16.a shows the results of the modelling and the experiments exemplified for several high-performing materials. Good match between the model and the machining data with the correlation coefficient of 0.96-0.99 indicates the applicability of the model for the description of the tool wear. However a slight underestimation can be observed on the initial engagement alongside with the minor overestimation at the end of tool engagement. The difference between the model and the experiments observed over the entire tool engagement is shown in detail on Fig. 16.b. Such behavior can be explained by the change in the conditions of the abrasion process during the cutting process. As mentioned earlier, the formation and retention of the TPL varies during the cutting. Initial formation of the TPL was observed during the first 500-1000 meters of engagement, while it attained the stable form after 2500-4000 meters, depending on tool material and cutting speed. More intense tool wear can be expected at the absence of TPL and therefore the model is likely to underestimate the wear rate. This means that the wear constant K used in the model changes its value as a result of variation tribologic conditions in the course of the test.

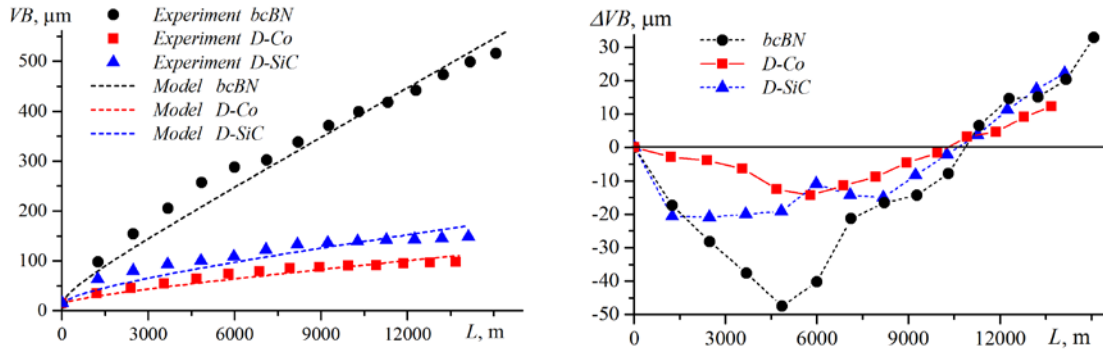


Fig. 16. (a) Modeling results for Archard wear model and (b) difference between model and experimental data for bcBN, D-Co, and D-SiC tools ($v_c = 400$ m/min).

Solution of Eq. 4 with respect to the wear constant K , as shown below (Eq. 5), allows for determination of such variation of its value for given test and tool wear conditions.

$$K = \frac{H_{tool} \cdot VB \cdot (VB - r_\beta) \cdot \cos(\alpha) \cdot \sin(\alpha)}{2 \cdot e \cdot (N_{22} + N_{21} \cdot VB)} \quad \text{Eq. 5}$$

Fig. 17.a shows that K value, and thus the wear resistance of the tool material, initially decreases and eventually approaches some asymptotic value upon longer tool engagement. The tool run-in and stabilization of TPL are related to this initial period. Fig. 17.b presents the average value of K over the entire cutting process. This value characterizes the tribologic wear conditions, irrespectively of the hardness of the tool material H_{tool} , and therefore can be used for judgement of the wear process itself. For example D-Co and B₆O-cBN tool materials have similar K value for tests at $v_c = 400$ m/min and in both cases the edge radius r_β (Fig. 8.b) for the worn tools and the dimensions of TPL are similar too.

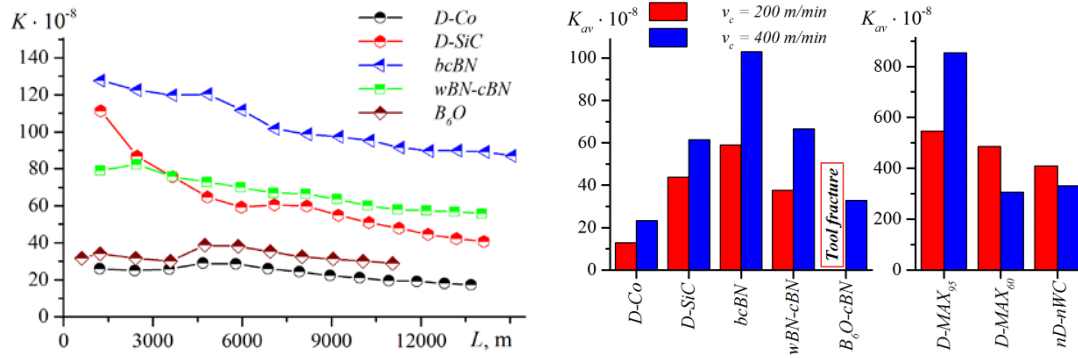


Fig. 17. (a) Variation of wear coefficient K during machining process ($v_c = 400$ m/min) and (b) average value of coefficient K for different tool materials.

3.3. Wear mechanisms

Removal of the tool protection layer by etching prior to 3D optical microscopy revealed additional features of the wear process. Post-etching reevaluation of the tool wear with SEM (Fig. 18.a) have shown that for D-Co and D-SiC tools a layer remains attached to the tool surfaces, even after prolonged etching. EDX analysis of the chemical composition of this layer has shown that the main constituents are Si and C, and also contains minor quantities of Al and O (see Fig. 18.b).



Fig. 18. (a) SEM close-up view of worn D-Co insert ($v_c = 400$ m/min) after etching, (b) EDX spectrum for layer adhered to the wear land.

A lamella for TEM analysis was prepared using FIB lift-out in order to fully study transition from TPL, through this etch-resistant layer, to the tool material. The flank wear land of a non-etched D-Co tool was chosen for this purpose. Fig. 19 shows SEM and TEM images of the interface between D-Co and TPL, where the lower part of the image is of the tool and the top part is the TPL. Scanning TEM (STEM) EDX analysis proved that the layer mainly consists of SiC with about 1 at% of O and 2 at% Al. Dark field TEM imaging (Fig. 19.b) demonstrates nano-structuring of the layer with the typical grain size of about 2-3 nm, with an upper limit of 10 nm. The very dense diffraction rings observed in the selected area electron diffraction patterns (Fig. 19.c) support the nano-structuring. The diffraction rings match the lattice spacing of zinc blende SiC {111}, {022} and {113} -planes, respectively.

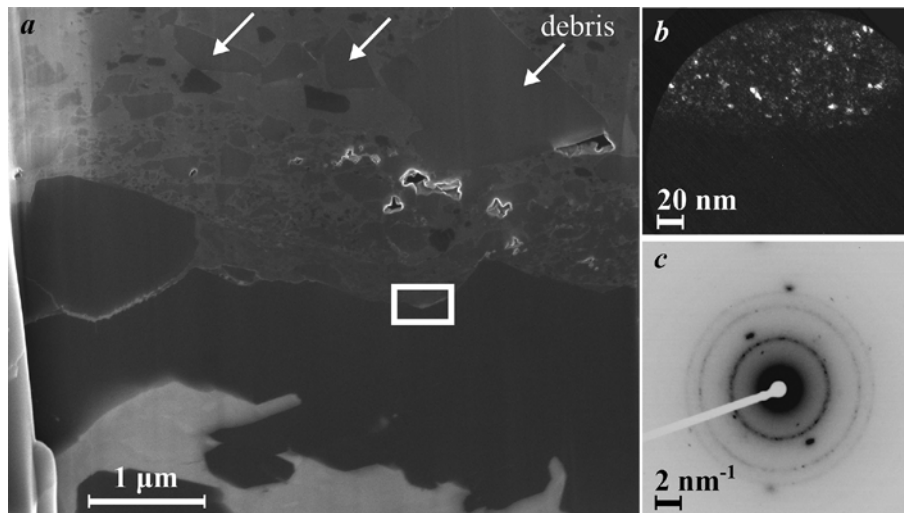


Fig. 19. (a) SEM image of the FIB prepared lamella and (b) dark field TEM image from the interface region between D-Co and TPL ($v_c = 400$ m/min). (c) SAED (inverted contrast) of the same region as in (b).

Presence of such SiC nano-crystalline layer, that is intimately attached to the diamond, implies chemical reaction between the diamond and elemental silicon from the MMC matrix material. The nano-structured reaction layer should not be confused with the micron-sized debris of SiC particles from the MMC, also observed on Fig 19.a. This observation indicates that the chemical wear mechanism plays an active role in the wear of diamond tooling.

Analysis of a similar FIB milled lamella extracted from the B₆O-cBN tool (Fig. 20) indicates absence of chemical interaction between tooling and MMC. In this case the TPL contains fine debris particles of eutectic Si, from the matrix of the MMC material, which are loosely located on the contact surfaces. Which is in opposition to the nano-crystalline SiC layer on D-Co that is intimately attached to the diamond. This indicates that not only the intensity of formation of the TPL is different between diamond and cBN-based tooling, but also the composition and attachment of the TPL is affected.

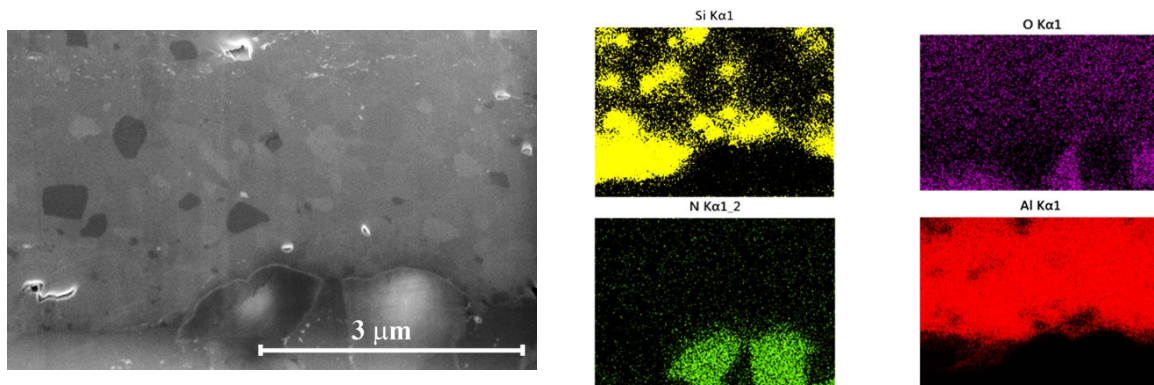


Fig. 20. EDX map of a sample FIB milled from the TPL on the crater of non-etched B₆O-cBN insert ($v_c = 200$ m/min).

The evidence for diffusion wear in D-Co tooling can be seen in Fig. 21.a which is depicting high angle annular dark field (HAADF) image of a crack in the D-Co tool, also visible on Fig. 19.a. From the STEM EDX elemental maps (Fig. 21.b) it is clear that Co is present in the majority of the crack. This indicates that the crack was formed in the presence of liquid Co, i.e. during sintering of the tool material. However, an approx. 0.5 μm long region of the crack opening (close to the TPL) did not bear any Co signal, instead, Al and Si was found in this region. Si is also present, to a lesser amount, throughout the rest of the visible crack. This clearly shows the diffusional removal of Co from the tool into the workpiece material, its replacement by Si and Al from the MMC matrix, and strong ingress of Si throughout the Co phase.

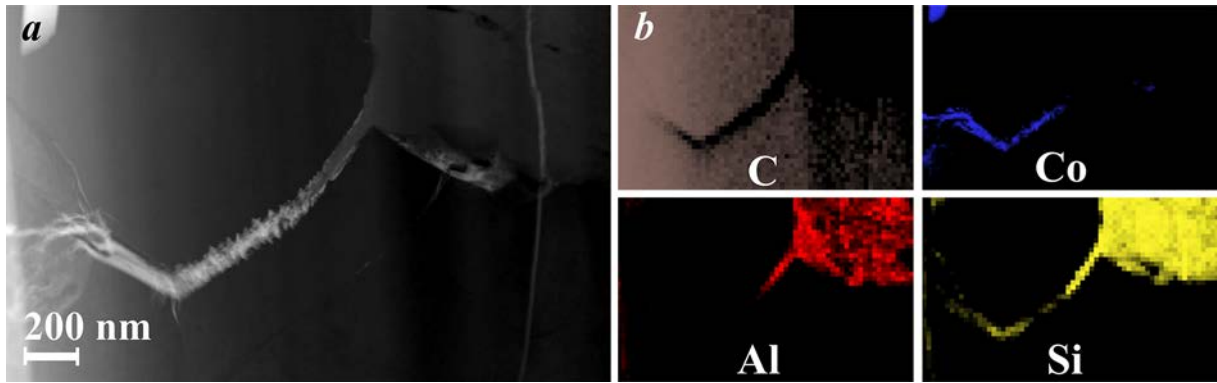


Fig. 21. (a) STEM HAADF image and (b) EDX elemental maps (C $K\alpha_{1,2}$, Co $K\alpha_1$, Al $K\alpha_1$, Si $K\alpha_1$) of a FIB lamella in the crack region of the D-Co tool ($v_c = 400$ m/min).

Another, more conventional, mechanism of tool material softening at high cutting speed and related high tool temperature is often attributed to the abrasive tool wear. This mechanism is often observed for cemented carbide tools which exhibit strong loss of hardness at elevated temperature. However in case of superhard tooling the situation is not as pronounced. Chou and Liu [21] have shown that machining Al-SiCp composite at cutting speed of 180 m/min results in the maximum temperature of 410 °C on the tool. The room temperature hardness (Fig. 3) of cBN-based tool materials decreases significantly and in this range of cutting temperature attains values of $HV \approx 22$ GPa for bcBN [22] and $HV \approx 20$ GPa for wBN-cBN [23] materials. Therefore SiC particles in the MMC having slightly higher hardness ($HV = 25-27$ GPa) [24] can inflict mild abrasive wear to the cBN-based tooling. In the case of diamond, its hardness reduces only to $HV \approx 84$ GPa for the given process temperature [24] and thus abrasion by the much softer SiC is very unlikely. On the other hand, the chemical wear of diamond tooling, which results in nano-structured SiC (Fig. 19), enables abrasive wear since the formed SiC is softer than diamond. Therefore chemical wear followed by abrasion of its reaction products is likely to be one of the primary wear mechanisms for diamond tooling. The kinetics of the chemical reaction is linearly proportional to the process temperature. In this case, temperature gradients along the flank wear land, with the highest temperature at the edgeline, would imply the intensity of SiC formation to decrease from the tool edge towards the end of VB, thus explaining negative clearance α_{VB} found only on diamond tooling (Fig. 7.a and Fig 8.a).

Another aspect of intensification of tool wear with the increase of cutting speed from 200 m/min to 400 m/min can be attributed to the reduction or destabilization (Fig. 11) of TPL, thus reducing its protective action. Andrewes et al. [25] argue that the higher hardness of diamond, compared to SiC, turns abrasive wear into a micro-mechanical damaging phenomenon, rather than micro-cutting one. Such mechanism of localized cracking and removal of the hard and brittle tool materials, similarly to the case of erosive wear [26], would explain the intensified wear rate observed at higher cutting speed. Formation and propagation of such localized cracks upon high energy impact of hard workpiece inclusions, such as SiC particles, is likely to intensify at high cutting speed. Indeed, Fig. 22.a shows evidence of cracking and partial removal of diamond grains from the rake surface of the worn D-Co tool and Fig. 22.b-c show evidence of a network of cracks forming in D-Co tool during the metal cutting. Co is expected to be found in all cracks formed during the tool liquid state sintering, while any cracks formed during metal cutting are expected to lack Co signal. In the high magnification image and elemental maps (Fig. 22.b-c) three cracks are visible, all connected to the major crack displayed in Fig. 21. The three cracks contain Si whereas only one contains Co, indicating that two were formed during cutting, in the absence of liquid Co. Loss of Co due to diffusional wear (Fig. 21) is expected to reduce the bonding and facilitate the cracking and breakage of diamond grains. It is expected that reduction or removal of TPL at high cutting speed of $v_c = 400$ m/min for all tooling leads to a higher intensity of SiC particles impacts and thus to accelerated tool wear.

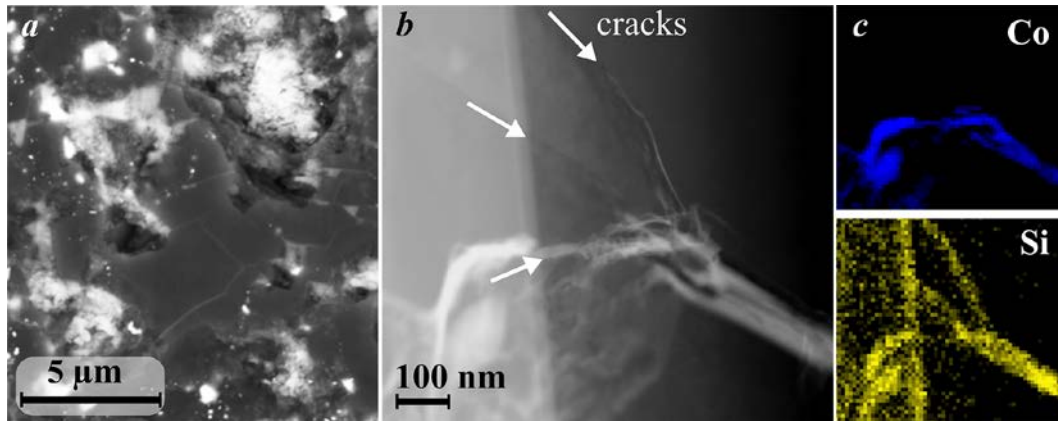


Fig. 22. (a) SEM image of cracking and fracturing of diamond grains on the rake of D-Co ($v_c = 200$ m/min), (b) STEM HAADF image of the crack network in D-Co ($v_c = 400$ m/min) and (c) EDX elemental maps (Co $K\alpha_1$, Si $K\alpha_1$) of the same region.

Even though TPL has a positive effect on the tool life, its excessive formation is the cause of built-up edge (BUE) as shown on Fig. 23.a. In case of B_6O -cBN and wBN-cBN superhard tool materials such excessive BUE resulted in seizure of the chips to the tool (Fig. 23.b), which eventually lead to rake flaking (Fig. 4.a and Fig. 9.a) and edge chipping.

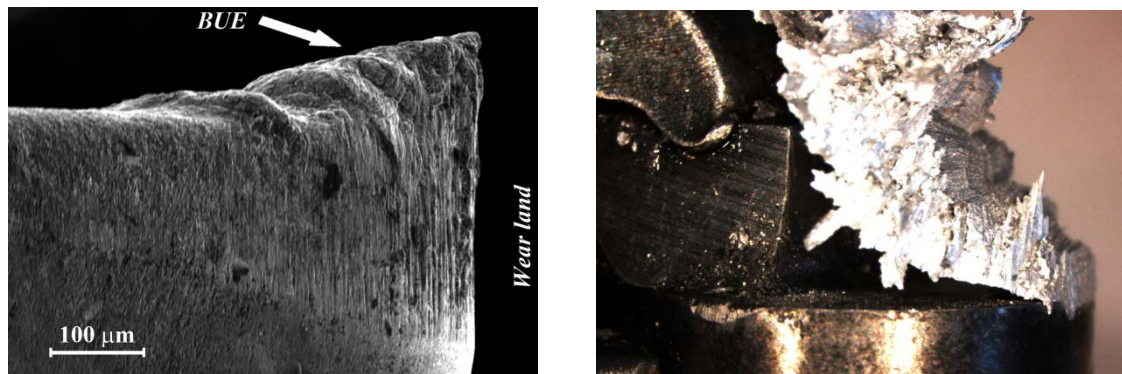


Fig. 23. (a) SEM image of build-up edge on the D-Co tool ($v_c = 200$ m/min) and (b) optical image of seizure of the chips to the rake of B_6O -cBN tool ($v_c = 200$ m/min).

Consequently chemical wear of diamond and subsequent abrasion of newly formed SiC reaction products, alongside cracking, fracture and removal of diamond fragments facilitated by diffusional wear of cobalt are governing the wear of diamond tooling. For cBN tooling, the reduced hardness at elevated temperature of the cutting process makes a mild abrasion possible, which was found to be the main wear mechanism. The protective action of TPL in all cases only retards the tool wear caused by abrasion and micro-mechanical damage.

3.4. Surface integrity

Formation of BUE, apart from its direct effects on the tool life and tool wear, negatively affects the roughness and integrity of the machined surface. Fig. 24 shows that the obtained roughness in all machining cases was significantly higher than the theoretically calculated value. Only in the case of bcBN machining at speed $v_c = 400$ m/min, which is accompanied by the loss of TPL, the surface roughness approached the expected level. Machining at $v_c = 200$ m/min is characterized by surface roughness being approximately two times higher, for respective tool materials, than the surface quality at higher cutting speed. This is related to the decrease of BUE dimensions with increased cutting speed and follows previous findings [7].

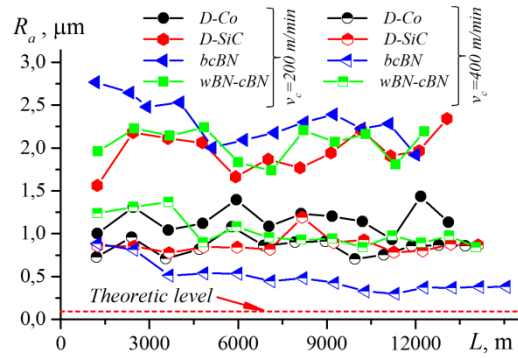


Fig. 24. Development of the surface roughness during the machining process.

The size of BUE, as shown on Fig. 23.a, is around 100 to 150 μm while the roughness in the respective case was only $Ra = 1.1 - 1.5 \mu\text{m}$. Cross-sectional analysis of the chips and the machined surface was performed in order to identify the cause of such difference. Fig. 25.a shows that the built-up edge predominantly remains with the chips while only a small fraction of BUE remains on the machined surface. It can be assumed that flank wear land of the tool additionally smoothens the machined surface after BUE breakage (Fig. 25.b), thus reducing its negative influence on the surface quality.

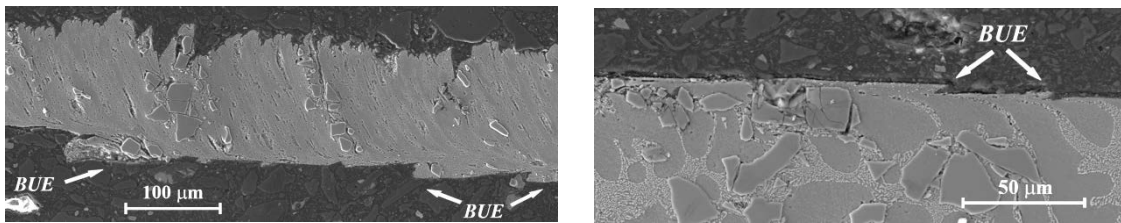


Fig. 25. SEM images of elements of build-up edge on (a) chips and (b) machined surface for D-Co tool ($v_c = 200 \text{ m/min}$).

On the other hand BUE is not the only source of increased surface roughness. Fig. 26.a shows that intensive SiC particle pluck-out in the course of the cutting process deteriorates the machines surface significantly. Fig. 26.b presents the details of the machined subsurface which reveal that fracture of the SiC particles by the incoming cutting edge and subsequent pluck-out of the SiC debris by the workpiece material adhered to the tool flank leaves pores and cavities, as deep as 10-20 μm , on the machined surface. Fig. 26.a also confirms that partial smoothing of the BUE remains over the machined surface by the tool flank.

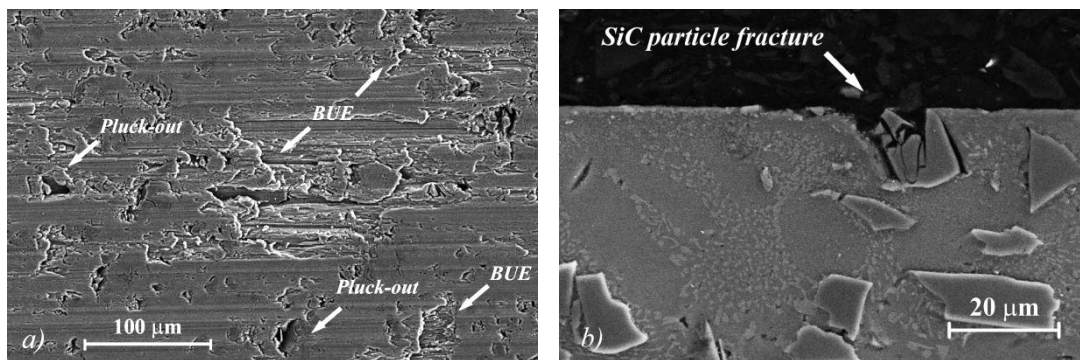


Fig. 26. SEM image of (a) machined surface and (b) subsurface with D-Co ($v_c = 200 \text{ m/min}$).

Conclusions

The current study addresses the issues of wear and performance of superhard diamond- and cBN-based tools when high speed machining cast Al-Si alloy reinforced with particulate SiC (20% vol.). The wear of the cutting tools was analyzed in detail using scanning and transmission electron microscopy. Archard-type model of abrasive tool wear was developed for modelling of tool deterioration and applied

for the analysis of all studied tool materials and machining conditions. The results of the analysis allow reaching the following conclusions:

- Tool materials, diamond with MAX-phase and nano-WC binders, possessing insufficient bonding exhibit low performance due to combined, adhesive and abrasive, wear.
- Adhesion of the workpiece material on the tool surfaces in the form of built-up layer or edge was found to demonstrate protective action against abrasion by SiC reinforcement, thus retarding tool wear. The dimensions and stability of this tool protective layer was found to decrease at higher cutting speed. Accelerated tool wear was observed in cases of destabilization and loss of TPL.
- SEM and TEM data confirmed chemical wear of diamond with formation of nano-structured SiC layer that is successively removed due to abrasion. Diffusional wear of cobalt was found on D-Co tooling, where it is replaced by Si and Al from the MMC matrix material. While abrasion of diamond by SiC particles was not identified, the high energy impact by the MMC reinforcement resulted in cracking and fracture of diamond grains.
- Presence of built-up layer and edge is shown to deteriorate surface finish. Machining at $v_c = 200$ m/min practically doubles the roughness compared to $v_c = 400$ m/min. However more significant damage to the machined surface is found to relate to fracture and pluck-out of SiC reinforcement by cutting tools.

Acknowledgement

This work was co-funded by Vinnova under “SICALight II. Lightweight components for automotive industry” project and under Strategic Innovation Programme for lightweight and metallic materials LIGHTer. It was also co-funded by the European Union’s Horizon 2020 Research and Innovation Programme under Flintstone2020 project (grant agreement No 689279). It is also a part of the strategic research program of the Sustainable Production Initiative SPI, involving cooperation between Lund University and Chalmers University of Technology. MMC workpiece material, alongside with valuable process information, was provided by Amtek Components Sweden AB. The authors would like to thank SECO Tools AB, Sweden for the help with commercial D-Co tooling, Dr. S. Nazarchuk from Institute for Superhard materials, Ukraine for supply of nD-nWC, as well as Prof. L. Jaworska from Institute of Advanced Manufacturing Technology, Poland for the supply of D-MAX₆₀ material. The cooperation research initiative between Institute for Superhard Materials (Ukraine) and Lund University (Sweden) is also greatly acknowledged.

References

- [1] Lin J.T., et al. Machinability of a silicon carbide reinforced aluminium metal matrix composite (1995) *Wear*, 181, pp. 883-888.
- [2] Hung N.P., et al. Cumulative tool wear in machining metal matrix composites. Part II: Machinability (1996) *Journal of Materials Processing Technology*, 58 (1), pp. 114-120.
- [3] Spriggs G.E. (2002) 13.5 Properties of diamond and cubic boron nitride. Beiss, P.; Ruthardt, R.; Warlimont, H. (eds.). Springer Materials—The Landolt-Börnstein Database.
- [4] Ciftci I., et al. CBN cutting tool wear during machining of particulate reinforced MMCs (2004) *Wear*, 257 (9-10), pp. 1041-1046.
- [5] Ding X., et al. Evaluation of machining performance of MMC with PCBN and PCD tools (2005) *Wear*, 259, 7–12, pp. 1225–1234.
- [6] Weinert K., König W. A Consideration of Tool Wear Mechanism when Machining Metal Matrix Composites (MMC) (1993) *CIRP Annals - Manufacturing Technology*, 42, 1, pp. 95-98.
- [7] Muthukrishnan N., et al. Machinability issues in turning of Al-SiC (10p) metal matrix composites (2008) *International Journal of Advanced Manufacturing Technology*, 39 (3-4), pp. 211-218.
- [8] Osipov A.S., et al. Drill bits with thermostable PCD inserts (2010) *Diamond Tooling Journal*, 2 (3), pp. 31-34.
- [9] Jaworska L., et al. Ti₃SiC₂ as a bonding phase in diamond composites (2001) *Journal of Materials Science Letters*, 20 (19), pp. 1783-1786.
- [10] Nazarchuk S.N., et al. Diamond-Tungsten Carbide Polycrystalline Composite Material (2011) *Journal of Superhard Materials*, 33 (1), pp. 1-12.
- [11] Petruska I.A., et al. Preventive action of silicon nitride at HT-HP sintering of cubic boron nitride (2015) *Journal of Superhard Materials*, 37 (4), pp. 222-233.
- [12] Bushlya V.M., et al. Tool wear and tool life of PCBN, binderless cBN and wBN-cBN tools in continuous finish hard turning of cold work tool steel (2014) *Journal of Superhard Materials*, 36 (1), pp. 49-60.
- [13] Isaev K.B., et al. Determination of the thermal conductivity coefficient of superhard materials (2003) *Powder Metallurgy and Metal Ceramics*, 42 (5-6), pp. 310-314.
- [14] Turkevych D.V., et al. HP-HT sintering, microstructure, and properties of B₆O- and TiC-containing composites based on cBN (2015) *Journal of Superhard Materials*, 37 (3), pp. 143-154.

- [15] Giannuzzi L.A., et al. Focused ion beam milling and micromanipulation lift-out for site specific cross-section TEM specimen preparation, (1997) MRS Proceedings, 480, pp. 19.
- [16] Bushlya V., et al. On the analytical representation of chip area and tool geometry when oblique turning with round tools. Part 2: Variation of tool geometry along the edge line (2015) Procedia CIRP, 31, pp. 423-428.
- [17] Archard, J.F. (1953) Contact and Rubbing of Flat Surface. Journal of Applied Physics, 24 (8), pp. 981-988.
- [18] Stahl J.-E. (2012) Metal cutting: models and theories. SECO: Fargesta, Sweden.
- [19] Zorev N.N. (1956) On the mechanics of metal cutting process. Mashgiz, Moscow, USSR.
- [20] Bushlya V., et al. On the analytical representation of chip area and tool geometry when oblique turning with round tools. Part 1: Chip area parameters under variation of side and back rake angle (2015) Procedia CIRP, 31, pp. 417-422.
- [21] Chou Y.K., Liu J. CVD diamond tool performance in metal matrix composite machining (2005) Surface and Coatings Technology, 200 (5-6), pp. 1872-1878.
- [22] Sumiya H., et al. Mechanical properties of high purity polycrystalline cBN synthesized by direct conversion sintering method (2000) Journal of Materials Science, 35 (5), pp. 1181-1186.
- [23] Bochko A.V., et al. Effect of structural factors on the ductility and strength properties of superhard materials based on boron nitride (1980) Soviet Powder Metallurgy and Metal Ceramics, 19 (5), pp. 368-374.
- [24] Mukhanov V.A., et al. Hardness of materials at high temperature and high pressure (2009) Philosophical Magazine, 89 (25), pp. 2117-2127.
- [25] Andrewes C.J.E., et al. Machining of an aluminum/SiC composite using diamond inserts (2000) Journal of Materials Processing Technology, 102 (1), pp. 25-29.
- [26] ElTobgy M.S., Ng E., Elbestawi M.A. Finite element modeling of erosive wear (2005) International Journal of Machine Tools and Manufacture, 45 (11), pp. 1337-1346.